New Journal of Chemistry

Electronic Supplementary Information (ESI)

Structural dependence of the optical properties of narrow band gap thiophene-thiadiazoloquinoxaline derivatives and their application in organic photovoltaic cells

Cristiana Costa [a,b], Joana Farinhas [a], João Avó [c], Jorge Morgado [a,d], Adelino M. Galvão[b,]*, Ana Charas[a,]*

1- Instituto de Telecomunicações, Instituto Superior Técnico, Av. Rovisco Pais 1, P-1049-001, Lisboa, Portugal.
2- Centro de Química Estrutural, Instituto Superior Técnico, Universidade de Lisboa, Portugal.
3- CQFM-IN and IBB-Institute for Bioengineering and Biosciences, Instituto Superior Técnico, University of Lisbon, Lisboa, Portugal.
4 - Department of Bioengineering, Instituto Superior Técnico, University of Lisbon, Lisboa, Portugal.

Contents

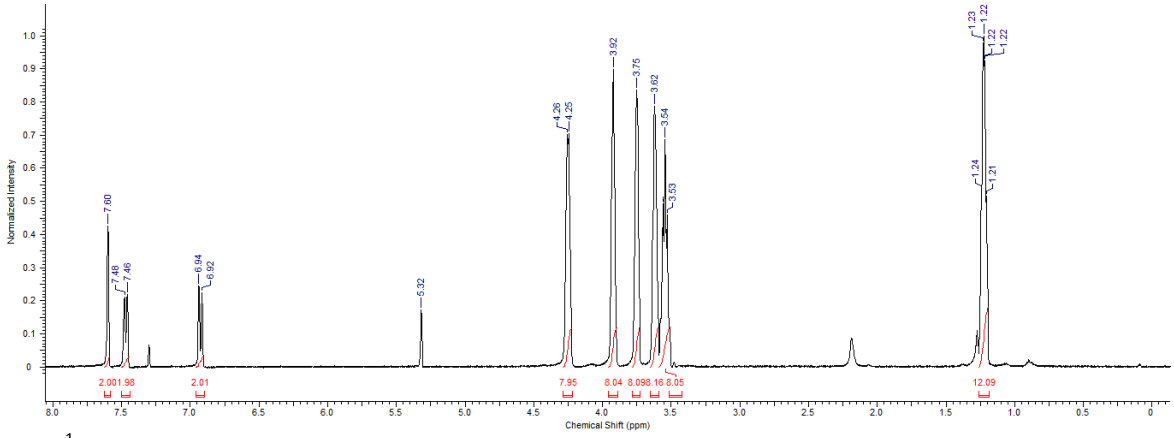

Figure S1. ^{1}H NMR (400 MHz) spectrum of 1,2-bis(3,4-bis(2-(2-ethoxyethoxy)ethoxy)phenyl)ethane-1,2-dione (3) in CD_2Cl_2.

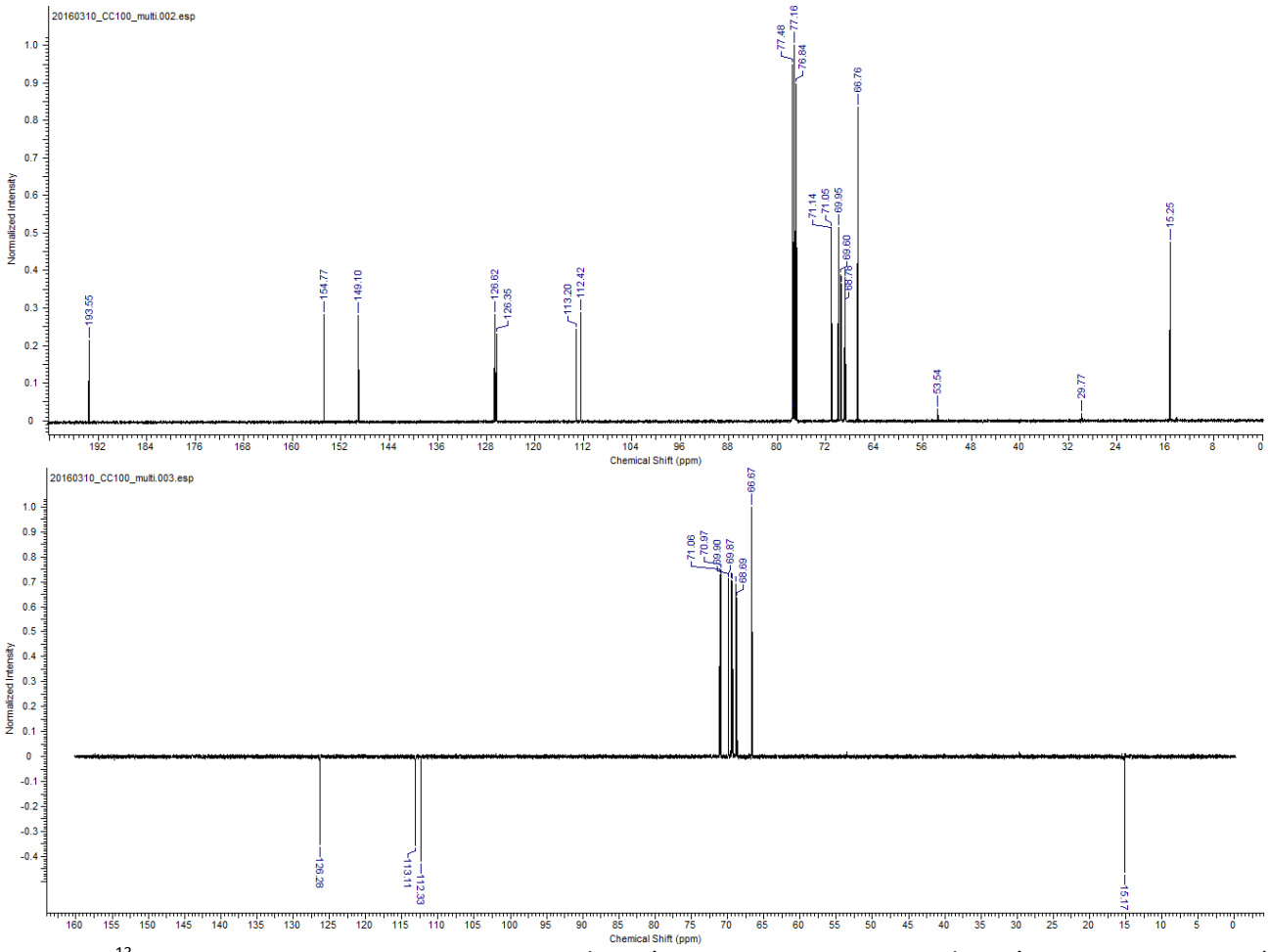

Figure S2. ^{13}C (100 MHz) (top) and DEPT 135 (CH and CH3's appearing negative and CH2's appearing positive) NMR spectrum (bottom) of 1,2-bis(3,4-bis(2-(2-ethoxyethoxy)ethoxy)phenyl)ethane-1,2-dione (3) in $CDCl_3$.

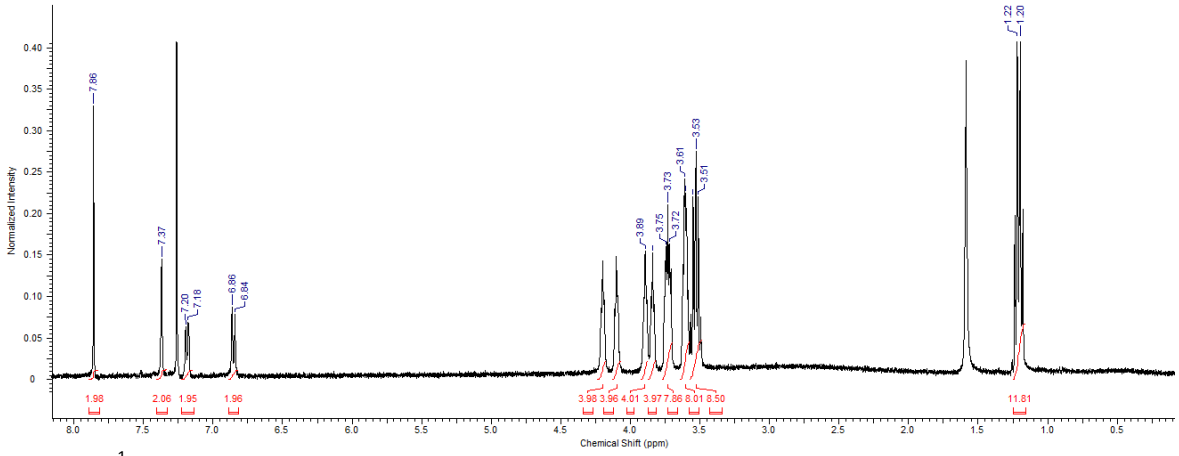

Figure S3. ^{1}H NMR (400 MHz) spectrum of 2,3-bis(3,4-bis(2-(2-ethoxyethoxy)ethoxy)phenyl)-5,8-dibromoquinoxaline (6) in $CDCl_3$.

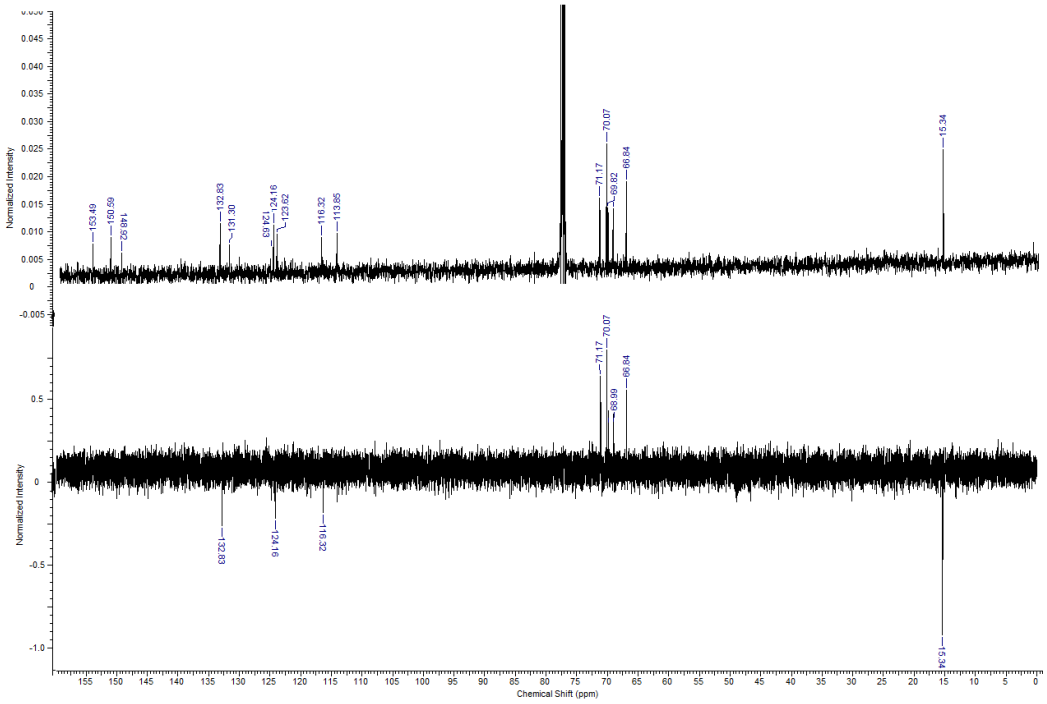

Figure S4. ^{13}C (100 MHz) (top) and DEPT 135 (CH and CH3's appearing negative and CH2's appearing positive) (bottom) NMR spectra of 2,3-bis(3,4-bis(2-(2-ethoxyethoxy)ethoxy)phenyl)-5,8-dibromoquinoxaline (6) in $CDCl_3$.

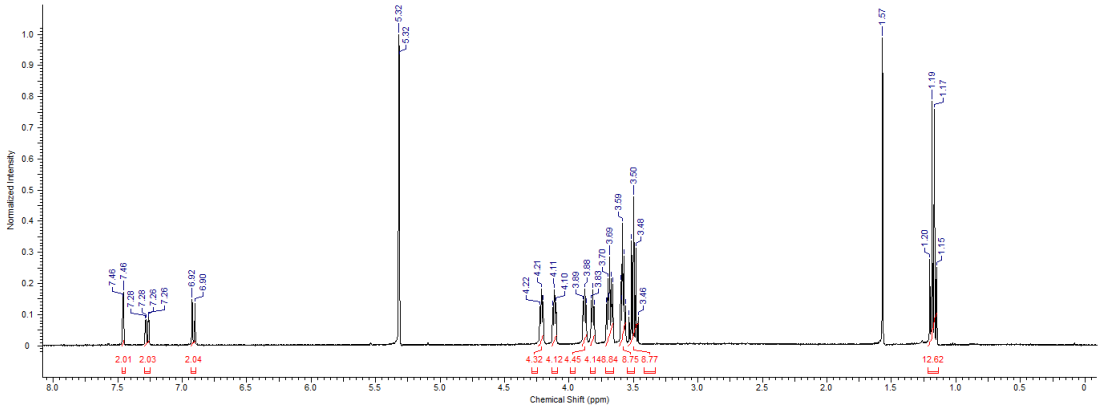

Figure S5. ^{1}H NMR (400 MHz) spectrum of 6,7-bis(3,4-bis(2-(2-ethoxyethoxy)ethoxy)phenyl)-4,9-dibromo-[1,2,5]thiadiazolo[3,4-*g*]quinoxaline (7) in CD_2Cl_2.

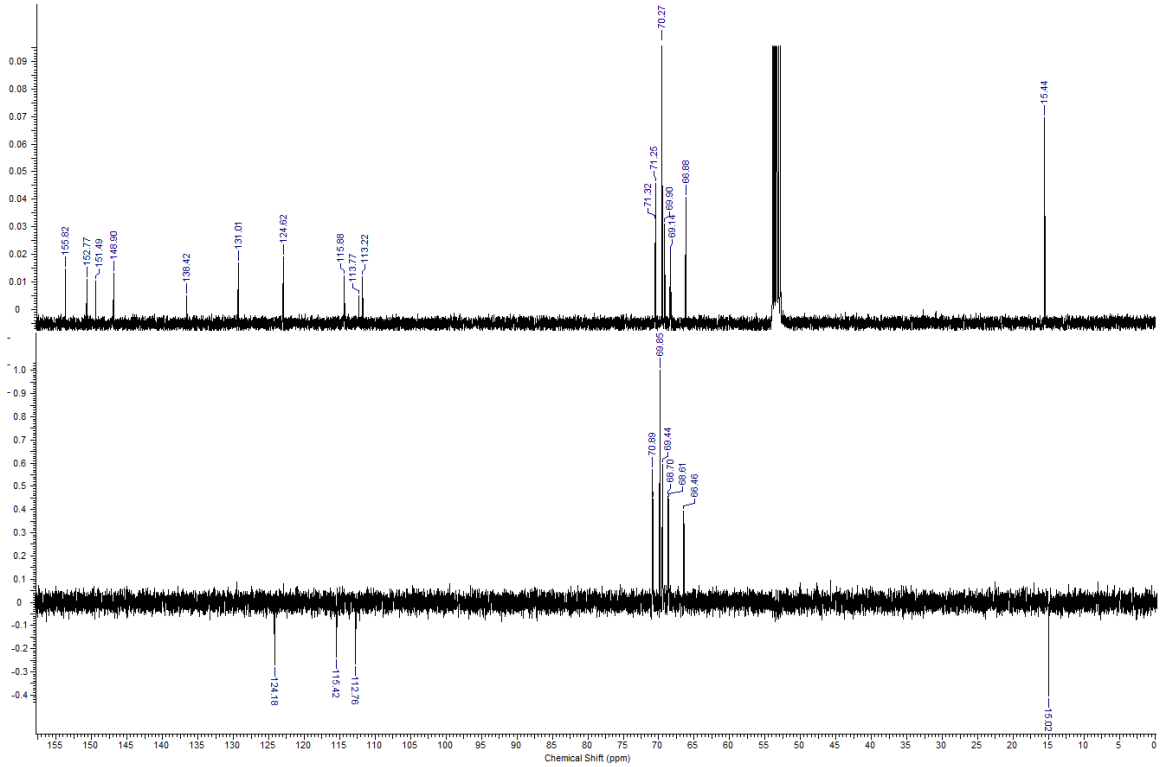

Figure S6. ^{13}C (100 MHz) (top) and DEPT 135 (CH and CH3's appearing negative and CH2's appearing positive) (bottom) NMR spectra of 6,7-bis(3,4-bis(2-(2-ethoxyethoxy)ethoxy)phenyl)-4,9-dibromo-[1,2,5]thiadiazolo[3,4-*g*]quinoxaline (7) in CD_2Cl_2.

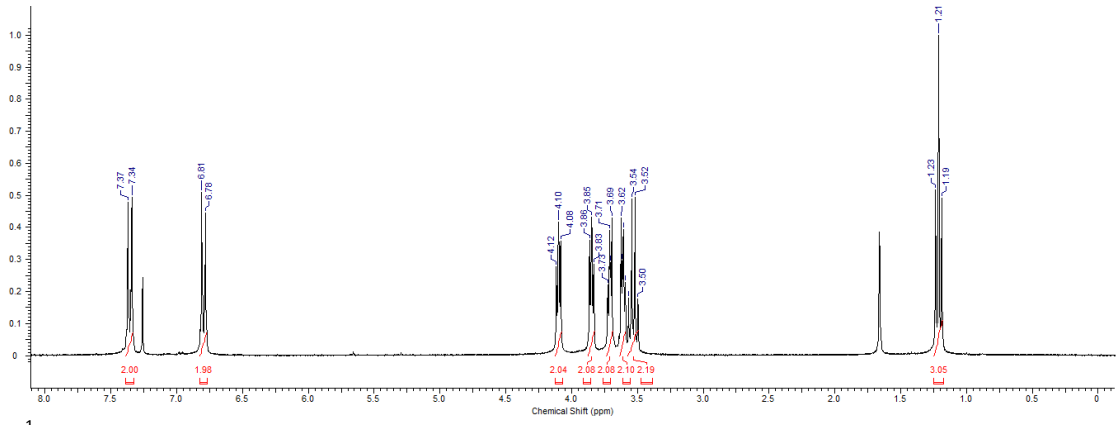

Figure S7. ^{1}H NMR (400 MHz) spectrum of 1-bromo-4-[2-(2-ethoxyethoxy)ethoxy]benzene (8) in $CDCl_3$.

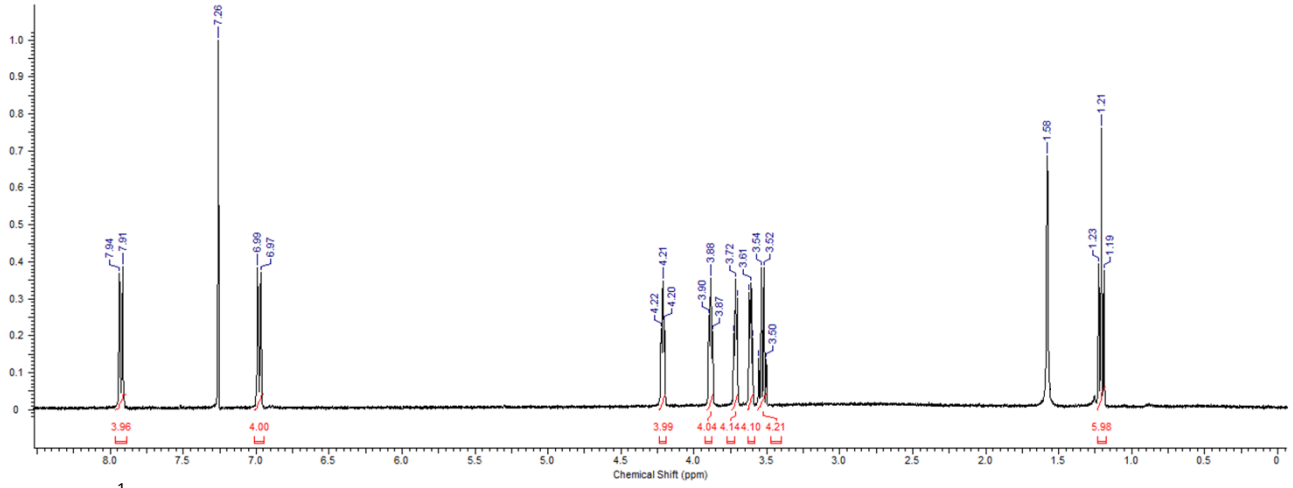

Figure S8. ^{1}H NMR (400 MHz) spectrum of 1,2-bis(4-(2-(2-ethoxylethoxy)ethoxy)phenyl)ethane-1,2-dione (10) in $CDCl_3$.

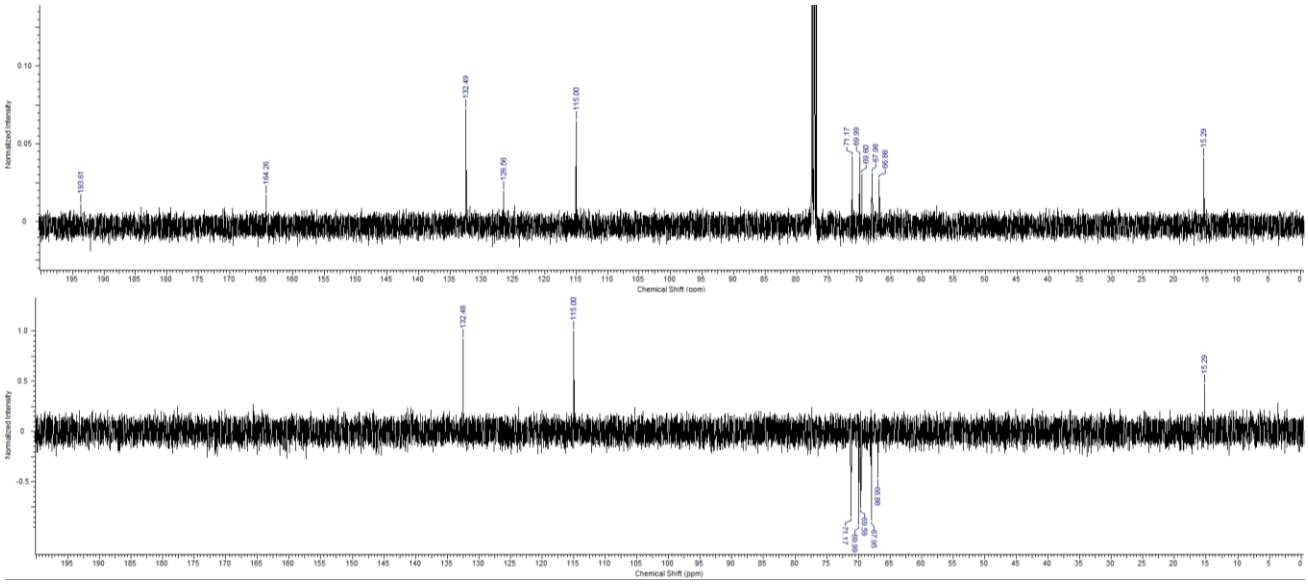

Figure S9. ^{13}C (100 MHz) (top) and DEPT 135 (CH and CH3's appearing positive and CH2's appearing negative) (bottom) NMR spectra of 1,2-bis(4-(2-(2-ethoxylethoxy)ethoxy)phenyl)ethane-1,2-dione (10) in $CDCl_3$.

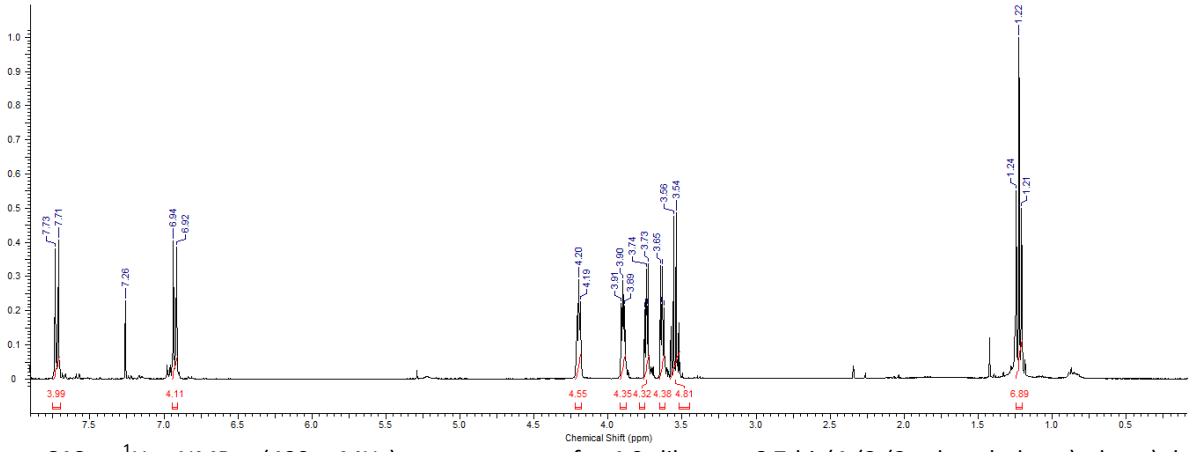

Figure S10. ^{1}H NMR (400 MHz) spectrum of 4,9-dibromo-6,7-bis(4-(2-(2-ethoxylethoxy)ethoxy)phenyl)-[1,2,5]thiadiazolo[3,4-*g*]quinoxaline (11) in $CDCl_3$.

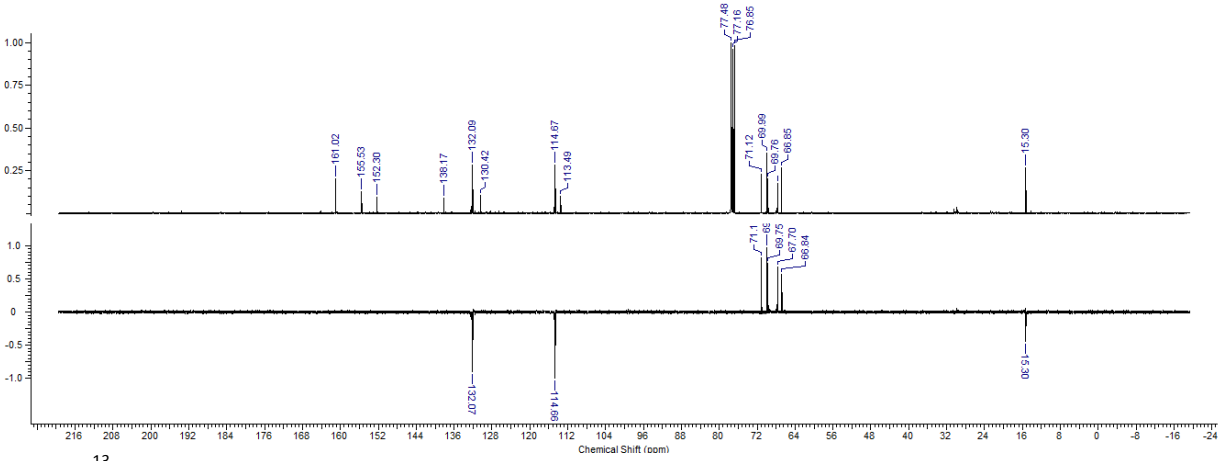

Figure S11. ^{13}C (100 MHz) (top) and DEPT 135 (CH and CH3's appearing negative and CH2's appearing positive) (bottom) NMR spectra of 4,9-dibromo-6,7-bis(4-(2-(2-ethoxylethoxy)ethoxy)phenyl)-[1,2,5]thiadiazolo[3,4-*g*]quinoxaline **(11)** in $CDCl_3$.

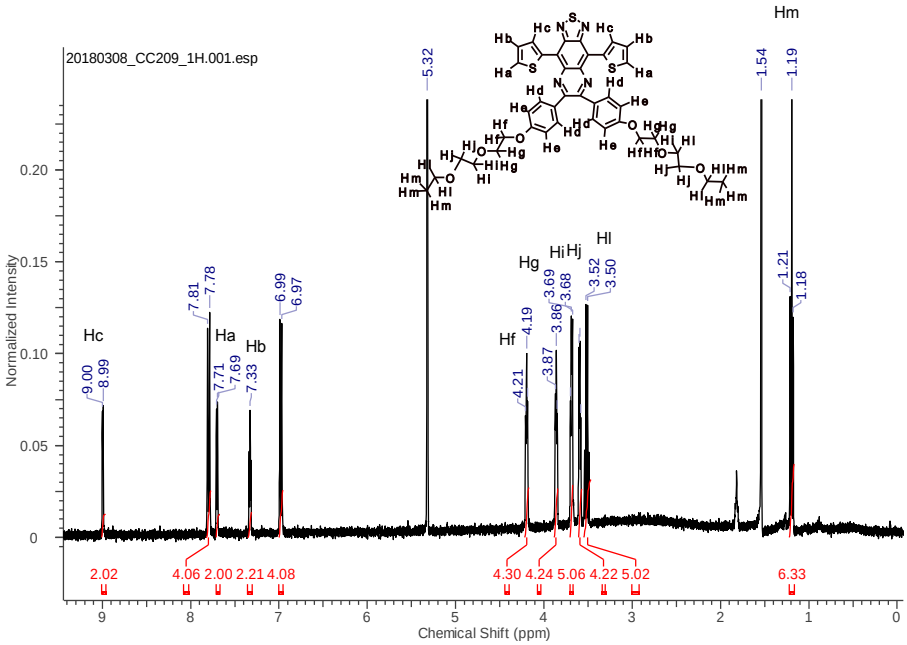

Figure S12. ^{1}H NMR (400 MHz) spectrum of TQT1 in CD_2Cl_2.

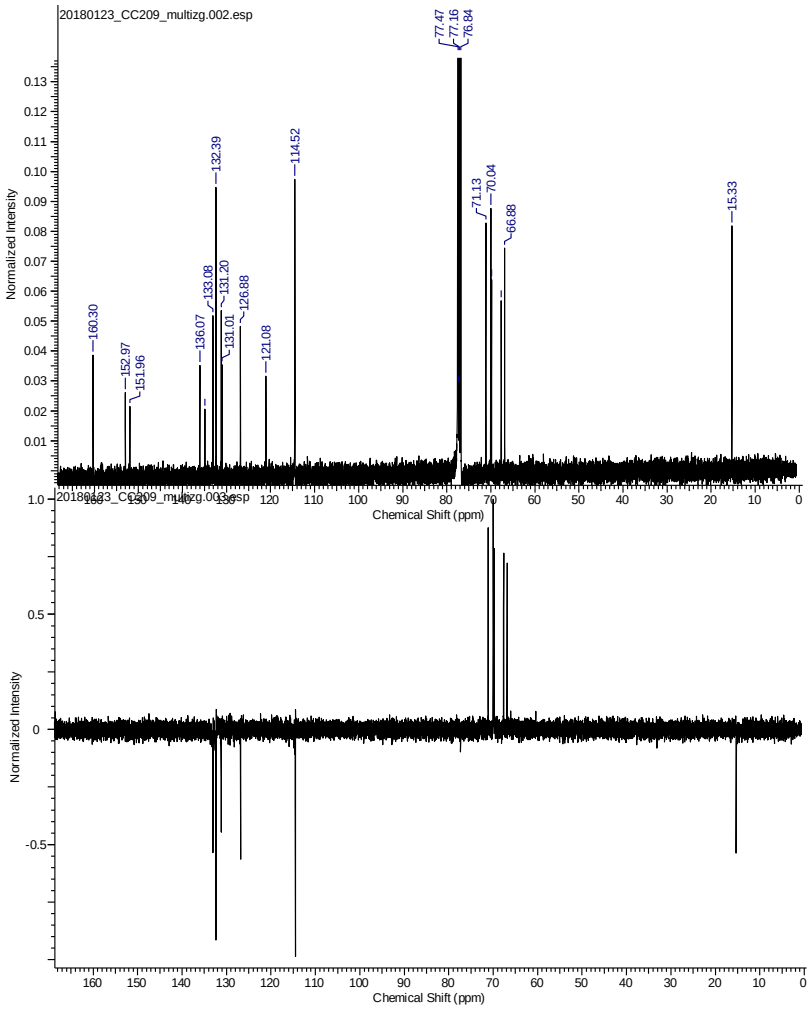

Figure S13. ^{13}C (100 MHz) (top) and DEPT 135 (CH and CH3's appearing negative and CH2's appearing positive) (bottom) NMR spectra of TQT1 in $CDCl_3$.

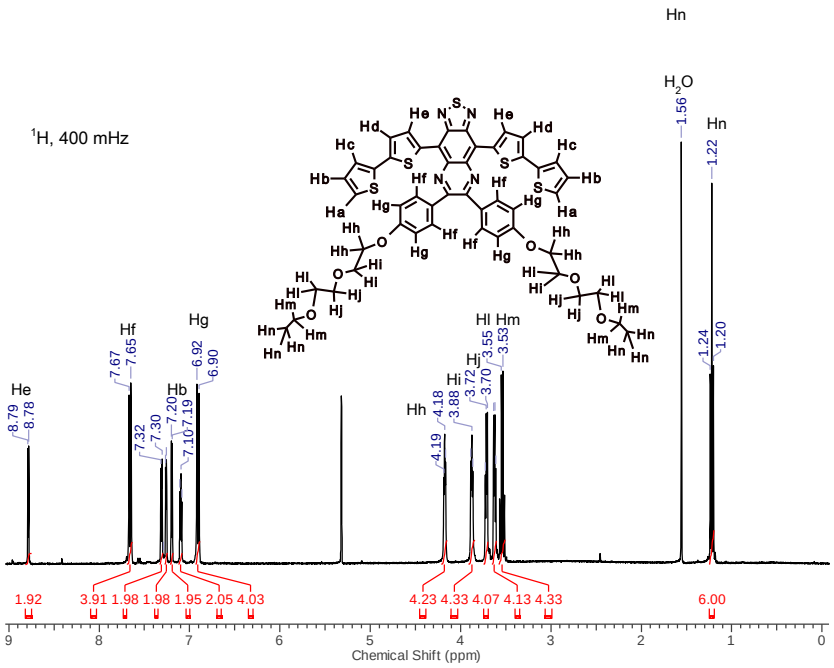

Figure S14. ^{1}H NMR (400 MHz) spectrum of TQT2 in CD_2Cl_2.

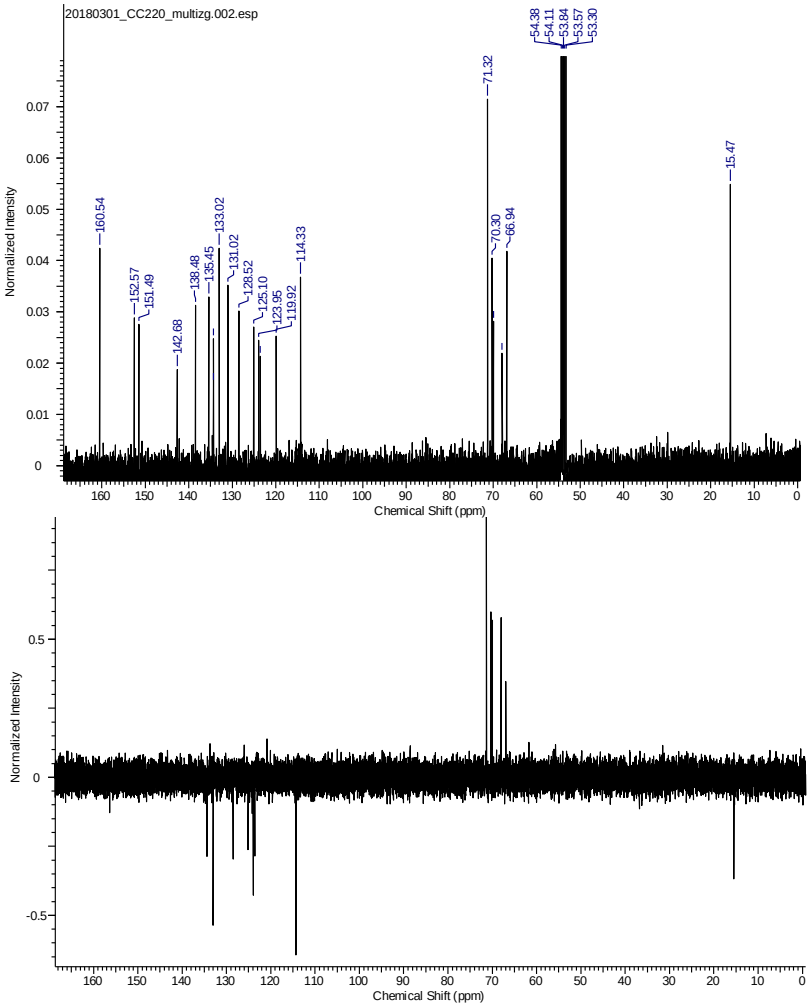

Figure S15. ^{13}C (100 MHz) (top) and DEPT 135 (CH and CH3's appearing negative and CH2's appearing positive) (bottom) NMR spectrum of TQT2 in CD_2Cl_2.

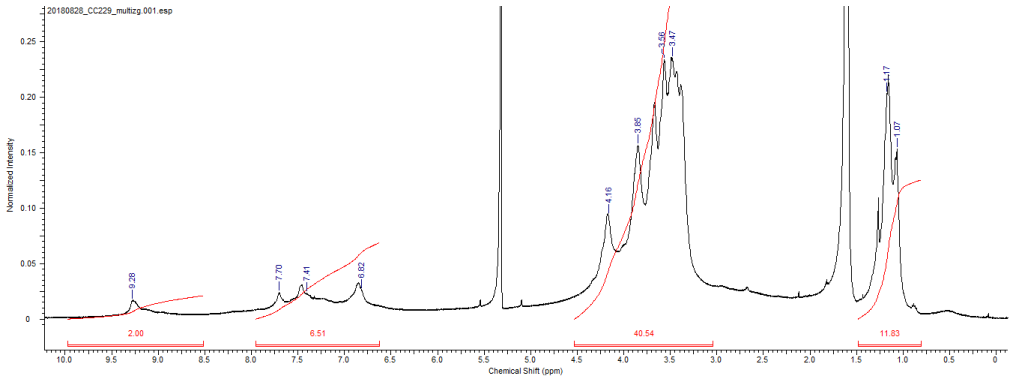

Figure S16. ^{1}H NMR (400 MHz) spectrum of PTQT in CD_2Cl_2.

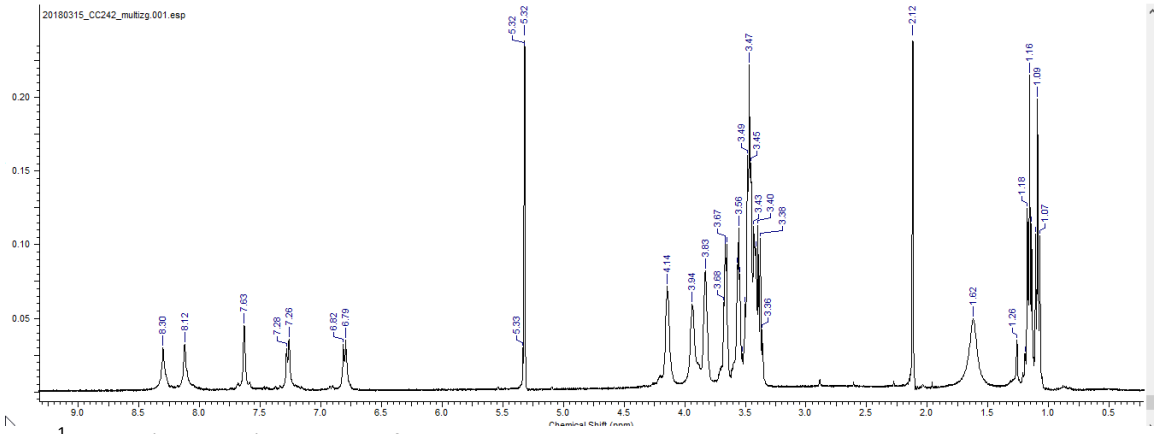

Figure S17. ^{1}H NMR (400 MHz) spectrum of PQT in CD_2Cl_2.

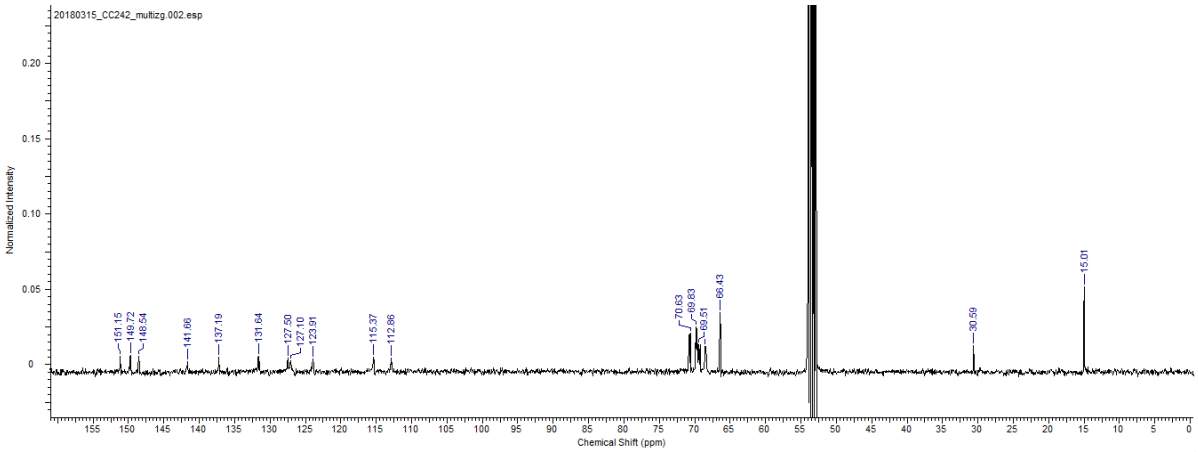

Figure S18. ^{13}C NMR (100 MHz) spectrum of PQT in CD_2Cl_2.

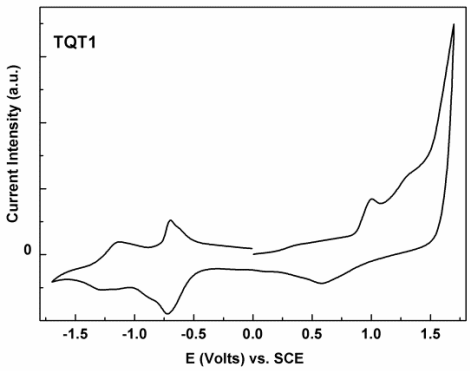

Figure S19. Cyclic voltammogram of TQT1 obtained at the scan rate of 50 mV/s.

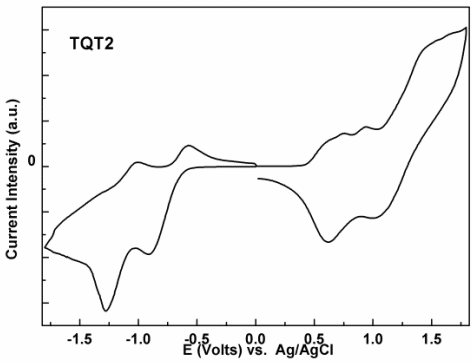

Figure S20. Cyclic voltammogram of TQT2 obtained at the scan rate of 50 mV/s.

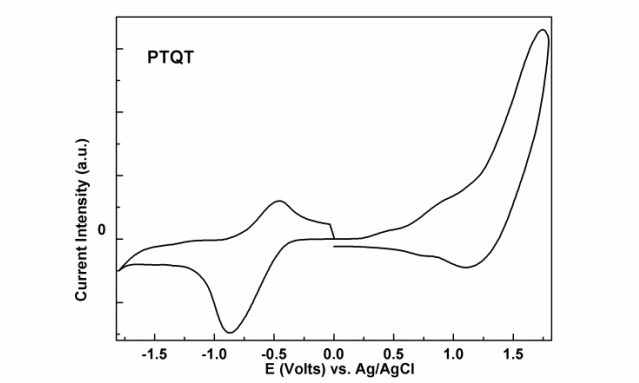

Figure S21. Cyclic voltamogram of PTQT obtained at the scan rate of 50 mV/s.

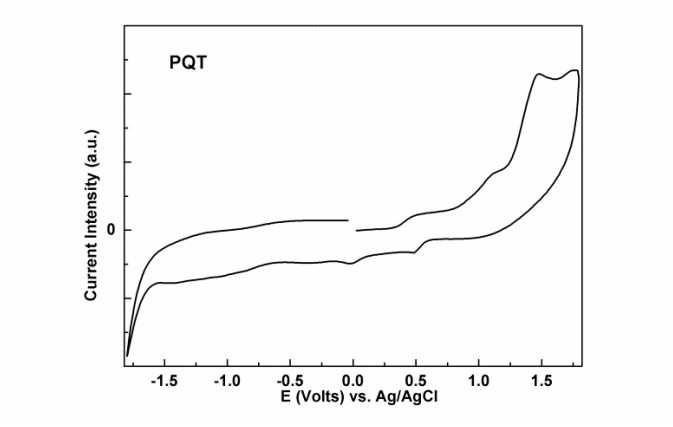

Figure S22. Cyclic voltammogram of PQT obtained at the scan rate of 50 mV/s

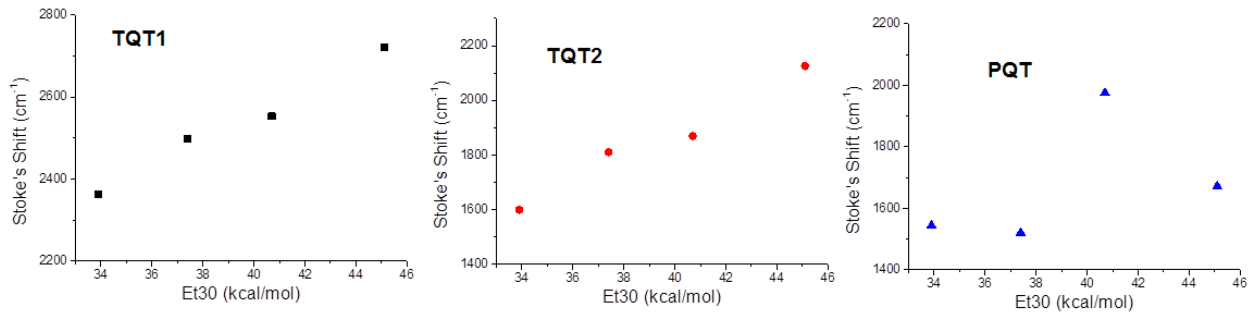

Figure S23. Stoke´s shifts as a function of the solvent polarity parameter Et30 for TQT1, TQT2 and PQT.

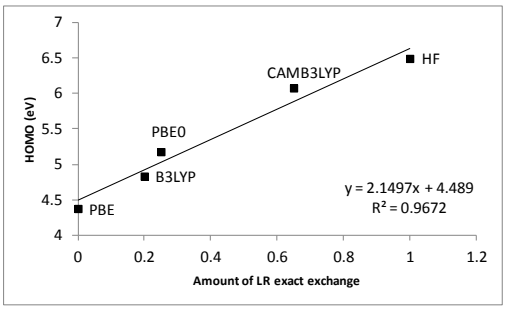

Figure **S24.** Dependence of the HOMO level on the amount of LR exact Exchange for **TQT1**

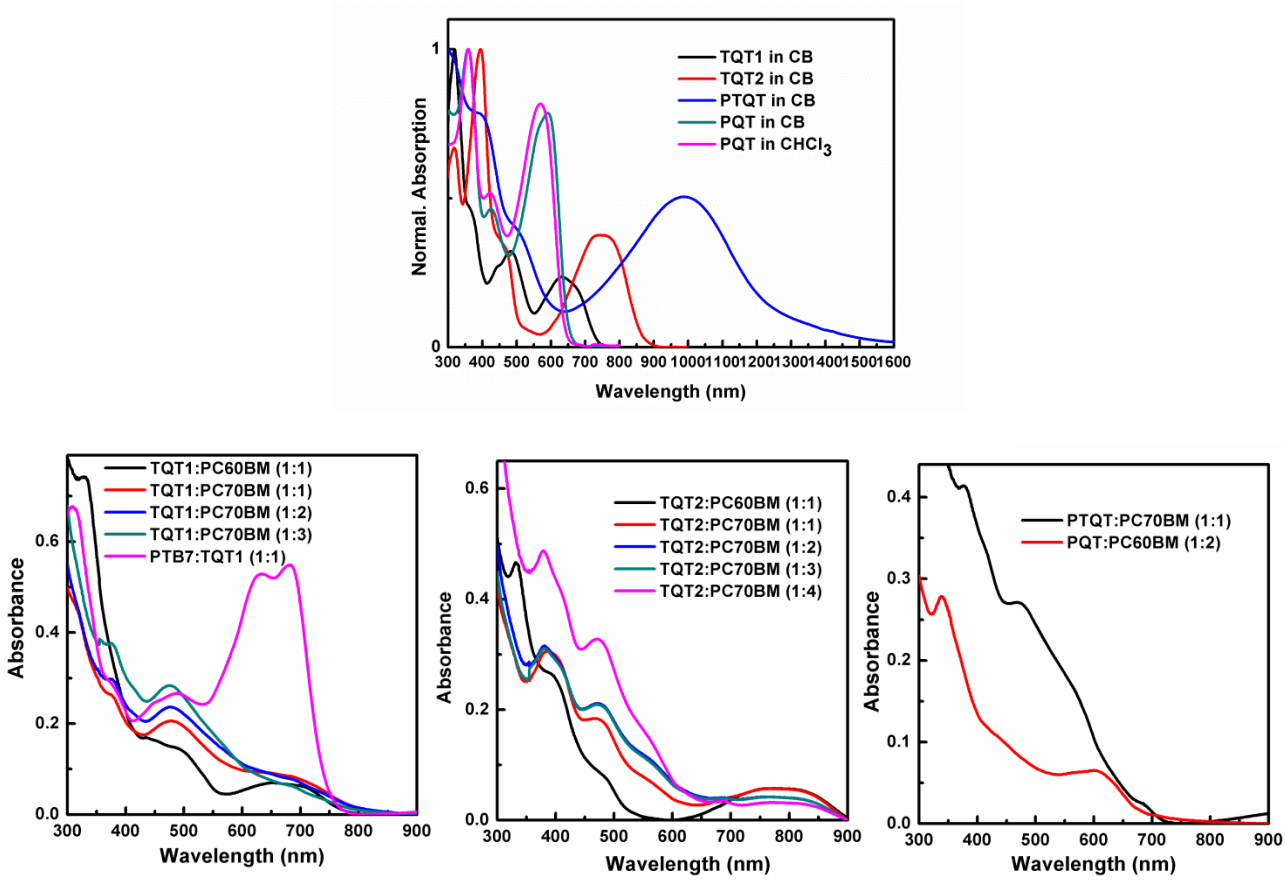

Figure **S25.** Top: UV-Visible absorption spectra (300-900 nm) of the pure compounds (TQT1, TQT2, PTQT, PQT) in the solvents used for preparing the active blends (chlorobenzene or chloroform) and (bottom) of active blends of the fabricated OSCs.

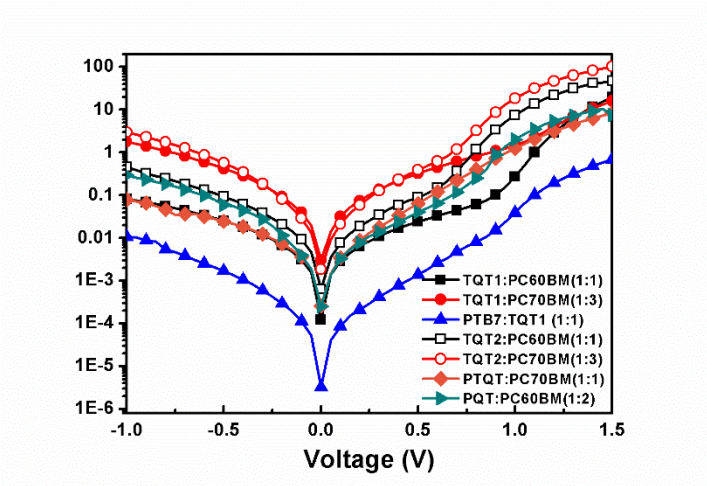

Figure S26. *J-V* curves in a semilogarithmic representation for the best performing OSCs for each D:A pair in the dark.

Table S1. Performance parameters of the solar cells fabricated with TQT1, TQT2, PQTQ, and PQT (under 82 mW.cm^{-2}).

Active layer	*Ratio (D:A)*	J_{SC} (mA/cm^2)	V_{OC} (V)	FF	PCE (%) best/ave[a]	Thickn (nm)
TQT1:PC$_{70}$BM	1:1	-1.20	0.81	0.23	0.29/0.24	90
	1:2	-2.16	0.88	0.21	0.51/0.46	85
	1:3	-2.93	0.88	0.27	0.88/0.70	90
TQT2:PC$_{70}$BM	1:1	-2.02	0.64	0.28	0.42/0.36	120
	1:2	-3.05	0.64	0.29	0.66/0.55	100
	1:3	-3.07	0.65	0.30	0.71/0.63	80
	1:4	-2.28	0.64	0.27	0.49/0.45	105
PTQT:PC$_{70}$BM	1:1	-0.33	0.24	0.21	0.02/0.02	150
PQT:PC$_{60}$BM	1:2	-1.17	0.82	0.48	0.61/0.54	95

[a] Best values followed by the averages calculated from at least 8 devices.

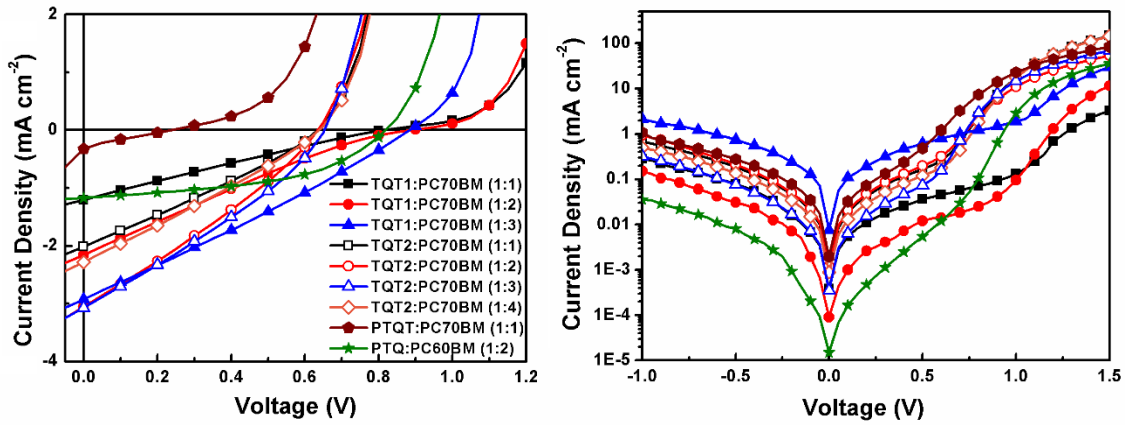

Figure S27. *J-V* characteristics for the OSCs under AM1.5G (82 mW/cm^2) illumination (left) and in dark conditions (semilogarithmic scale) (right).

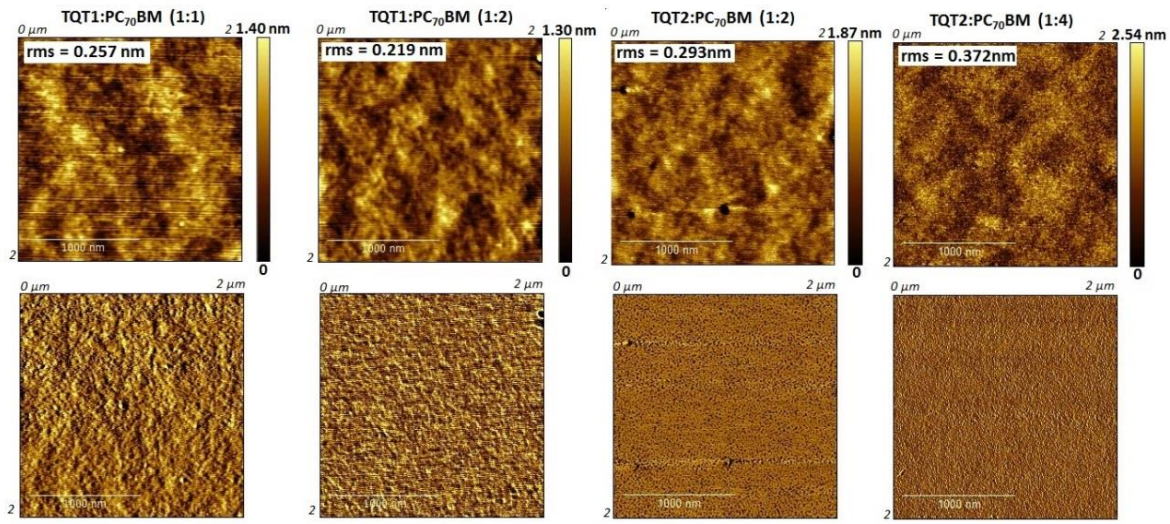

Figure S28. Phase AFM images of the active layers shown in Figure 6 of the main manuscript.

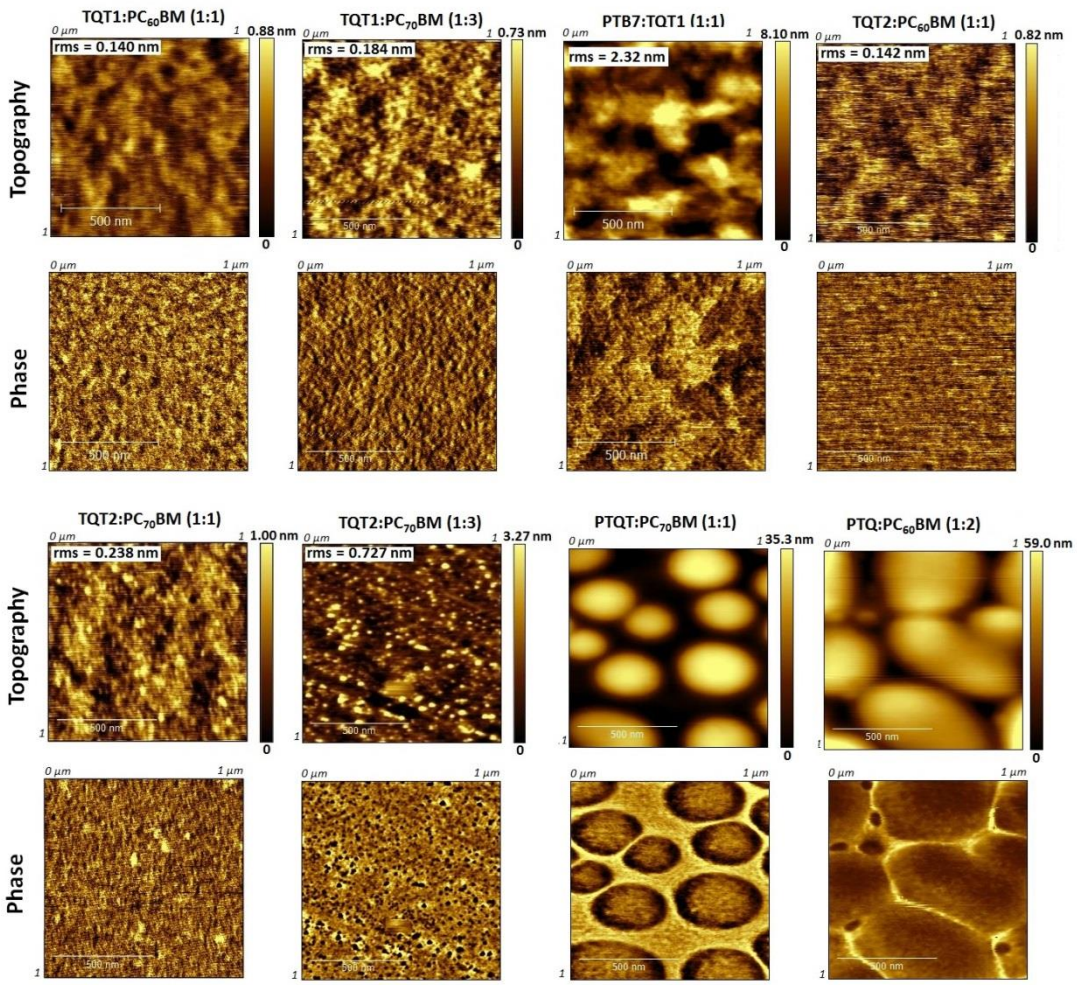

Figure S29. AFM images of active layers of the fabricated cells.